THE TORSIONAL AND SHEAR BEHAVIOR OF STEEL FIBER REINFORCED RC MEMBERS

Abdulkadir Cüneyt AYDIN [a]*, Mahmut KILIÇ [b], Mahyar MAALI [c], Barış BAYRAK [d], Erkan TUNÇ [e]

[a] Prof.; Ataturk University, Engineering Faculty, Department of Civil Engineering, 25030, Erzurum, Turkey
*Corresponding author. E-mail address: *acaydin@atauni.edu.tr*

[b] Assistant Prof.; Ataturk University, Engineering Faculty, Department of Civil Engineering, 25030, Erzurum, Turkey
E-mail address: *mahmut.kilic@atauni.edu.tr*

[c] Associate Prof.; Erzurum Technical University, Engineering and Architecture Faculty, Department of Civil Engineering, Erzurum, Turkey
E-mail address: *mahyar.maali@erzurum.edu.tr*

[d] PhD; Ataturk University, Engineering Faculty, Department of Civil Engineering, 25030, Erzurum, Turkey
E-mail address: *baris.bayrak@atauni.edu.tr*

[e] MSc; Ataturk University, Engineering Faculty, Department of Civil Engineering, 25030, Erzurum, Turkey
E-mail address: *rkntnc.06@gmail.com*

Abstract
Beams and columns are one of the important structural elements of buildings to take up transverse loads such as axial load, bending moment, shear, and torsion. Present work is an experimental investigation on the shear, torsion, and axial load behavior of the structural members like columns and/or beams. The reinforced concrete members with 0, 30, and 60 kg/m³ of steel fibers were tested for torsion, shear and axial loading for this study. The twist angle, the load-deflection behavior, the ultimate shear strength, the torsional moment, and the critical moments were obtained for the loading type and steel fiber ratios. The results show that the increasing steel fiber ratio, increased the torsional moment capacity and decreased the shear strength capacity. On the other hand, increasing the steel fiber content increased the both axial load and moment capacity of RC columns. The shear strength and the torsional moment capacities are defined by the provision of current codes of practice such as ACI318-19, Eurocode-2, British, Australian and Turkish Standards.

Keywords: Behavior; Interaction; Reinforced concrete; Shear; Steel fiber reinforcement; Torsion.

1. INTRODUCTION

Concrete is widely used structural material, all over the world. The excellent versatility, availability, and economy of the concrete makes it a pioneer of the construction industry when it is compared to other materials. Beams/columns are one of the main structural elements of building to respond to the effects, such as bending moment, shear, and torsion. Thus, it is important to investigate the relevant behaviors of

members [1, 2]. Steel fibers have been used to improve the characteristic properties of concrete in practice for many years. Besides the commercial use of fibers in concrete technology began in 1970s, particularly in Europe, Japan, and USA. In the structural application, concrete behaves as a brittle material with low tensile strain capacity and with some softening post-peak behavior in compression essentially due to the transverse strain capacity. The use of steel fibers in the

concrete matrix increases the low tensile strain capacity by controlling the micro and macro cracking [3–5]. There are also some advantages and disadvantages of use of steel fiber in concrete. Firstly, the use of steel fibers increases the tensile strength, ductility, and flexural toughness characteristics of the concrete. Moreover, the presence of steel fibers reduces the formation and propagation of cracks due to early age plastic settlement and drying shrinkage. Secondly, the brittle behavior of the concrete evaluates to tougher fracture mechanism [3]. On the contrary, the use of steel fiber has no meaningful effect on the compressive strength [6–8].

The addition of steel fibers in the concrete mix has long been recognized as non-conventional mass reinforcement that enhances the mechanical properties of concrete and provides for cracking propagation control [9]. The tensile stress transfer capacity of steel fibers across crack surfaces is defined as crack bridging and hence, shear across developing cracks are resisted by steel fibers. The energy dissipation capacity of structural element increases, relative to the brittle failure of the concrete as for the tensile strength [10]. Furthermore, the steel fibers also increase the torsional strength, the tensile strength, stiffness, toughness and ductility [9, 11–14].

The torsional moment in structures occurs when resultant force acts eccentrically relative to the longitudinal axis of an element [15]. For many years, torsional moment was not regarded in the process of design of structural members, but the studies in recent years showed that the torsional strength must be considered to subject the eccentrically loaded structural members [16]. Researchers especially focus on bending moment/shear forces when designing structural members. Thus, the torsional moment is neglected in some cases. Torsion can be an important problem for structural members such as eccentrically loaded beams, spandrel beams and curved girders, etc. [17]. The torsional behavior of the member is different from the shear behavior due to diagonal tension cracks that occur on the two sides of structural element. The cracks occurred due to shear force propagate in the same direction on both sides of the structural member, in which the cracks occurred due to torsion propagation of a spiral pattern, propagating in opposite directions on the opposite sides of the beam [18]. Thus, to prevent the crack propagation must be provided according to code [19–21]. The investigation of torsional behavior of reinforced concrete (RC) members has been started at the beginning of the last century. In earlier, the plastic and elastic theories were used to predict the behavior of RC members under torsional moment. However, these two theories remained incapable for torsional behavior of the member due to their deficiency. In recent decades, two main theories have been focused on by researchers to calculate torsional moment capacity, namely the skew-bending theory that was based on the American code between the 1971 and 1995, and the space truss analogy, which was the base of American code since 1995 and of European code since 1978 [22]. A structural element subjected to the pure torsion is characterized by the behavior of the element in direct tension. Hence, the poor properties of concrete such as tensile strength must be improved by new ways or materials. Another innovative concept to improve the tensile strength of the concrete is to add steel fibers into the plain concrete mixture. The cracking of reinforced concrete elements is a natural process due to tensile strength of concrete. Thus, the crack propagation cause the adverse effect on the structure's serviceability and durability [15]. In addition, the formulas for calculating cracks of the member subjected to pure torsion or bending moment is not defined in any standards or codes. Hence, to comment and to understand the cracks is very important issue for researchers.

The interaction diagram is commonly used to determine the strength capacity of the structural members, especially for RC columns. The RC columns can be designed by calculating axial force and moment values from the interaction diagram. The interaction diagrams are usual tools for RC cross-section analysis and design. The interaction diagrams are plotted to use the ultimate values of the bending moments and axial force for evaluating the cross-section strength [23, 24]. The interaction diagrams present a widely used practical tool for the design of RC structures, which is selected for a few reasons including their ability to contribute a favorable graphic of the ultimate axial force and moment capacity of structural members. There are characteristic points that are defined corresponding to the strain limitations relating to reinforcing steel in tension and concrete in compression [25]. The interaction diagrams used to design RC members are based on the several assumptions. Firstly, a maximum allowable concrete compressive strain prevents concrete crushing. Secondly, the plane sections remain plane, the tensile strength of concrete is negligible and the concrete stress distribution can be represented by a rectangular stress block [26].

The aim of this study focuses on the axial loading, the

torsional, the shear, and the flexural behaviors of steel fiber reinforced RC members. The experimental program reported in this paper included not only three (3) beams with rectangular section under pure torsion, but also seven (7) beams with rectangular section, subjected to bending moment. On the other hand, the axial load was applied on twelve columns. The experimental program is consisting of three groups of specimens. The first group includes the conventional RC members as control specimens. The second group of members include the RC members with 30 kg/m^3 steel fibers. The last group consists of the RC members with 60 kg/m^3 steel fibers. As an experimental work, the three-point bending, four-point bending, and overhanging beam type loading systems are realized. These experiments are designed to investigate the axial, the torsional, the shear, and the flexural behavior of the RC members.

The experimental data presented in this paper provide valuable information on understanding the strength and behavior of RC beams and columns with steel fibers under pure torsion, three different types of loading and axial force. The free end deflection, mid-span deflection, flexural strength, torsional moment-rotation, critical torsional moment, crack propagation, axial load capacity and the interaction diagrams of the members are evaluated.

2. EXPERIMENTAL SETUP

2.1. Specimen details

A set of ten rectangular 1500 mm length beams were tested up to the failure. The beams have same square cross-section. The dimensions of the tested beams were chosen as 200x200x1500 mm and longitudinal and transverse reinforcement were designed according to the Turkish Code 2018 [21] and ACI318-19 [19]. The concrete type, dimensions of the tested members, stirrups and the longitudinal reinforcements and concrete cover (distance from the center of longitudinal rebar to cross section outer face-30 mm) keep the same for all beams. Table 1 presents a summary of the properties of the tested beams. The longitudinal reinforcement is 2Ø14 (i.e. 2 bars 14 mm diameter) at the bottom of the beam and 2Ø14 at the top of the beam. The stirrup reinforcement was designed to be as Ø8/200 mm (i.e. 8 mm diameter stirrup for every 200 mm) at the center section and Ø8/100 mm at the top of beam. The geometry and reinforcement design details are presented in Fig. 1a. The longitudinal and stirrup reinforcements were ribbed steel. Three of both longitudinal and stirrup

reinforcement details were tested under the laboratory condition, and the average of these values was calculated. The yielding strength (f$_{yd}$) for the steel rebars were 420 MPa. The stress-strain curves of are presented in Fig. 2.
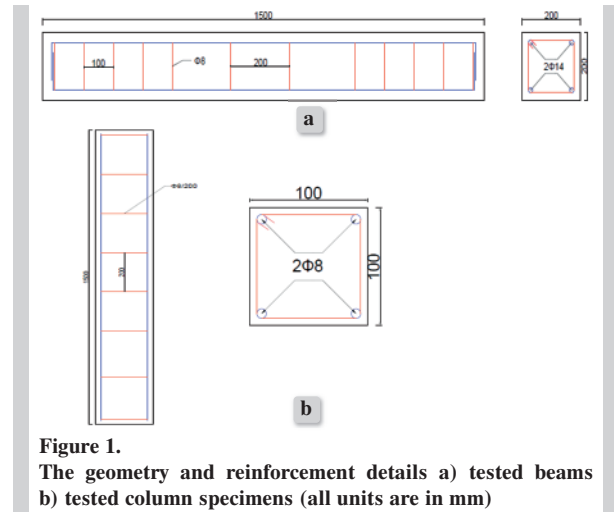

Figure 1.
The geometry and reinforcement details a) tested beams b) tested column specimens (all units are in mm)

The dimensions of the tested columns were chosen as 100x100x1500 mm and were designed longitudinal and transverse reinforcement according to the Turkish Code 2018 [27] and ACI318-19 [28]. The cross sections are considered according to laboratory conditions, also. The concrete type, dimensions of the tested columns, stirrups (8 mm diameter stirrup for every 200 mm) and longitudinal reinforcements (2 bars 8 mm diameter at the bottom and 2 bars 8 mm at the top of the column) and concrete cover (10 mm) were kept same for all columns. The twelve RC columns were manufactured: four reference specimens without fiber, four specimens with 30 kg/m^3 fiber, and four specimens with 60 kg/m^3 that applied axial load with 0, 10, 20 and 30 mm eccentrically. The geometry and reinforcement details of the columns were shown in Fig. 1b. The longitudinal and stirrup reinforcement of the columns were symmetric, and the yielding strength (f$_{yd}$) was 420 MPa. The stress-strain curves of both longitudinal reinforcements and stirrups are presented in Fig. 2.

The tested beams were sorted into four groups named as T, FC, F3, F4 and the tested columns were sorted in one group named as AL based on their loading type. Each group was divided into three categories. The groups, T and FC, include 3 beams: with one conventional concrete without fibers, with two 30 and 60 kg/m^3 steel fibers under torsion (T), overhanging (FC) respectively. The groups, F3 and F4,
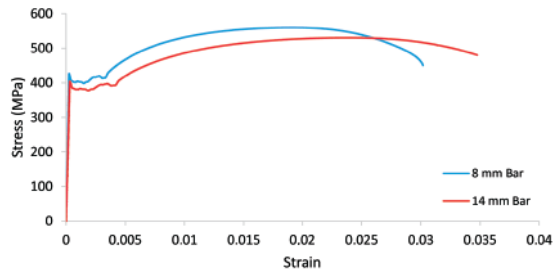
Figure 2.
The stress-strain curves of the reinforcements

Table 1.
Summary of tested specimens

Specimens	Steel Fibers (kg/m³)	Loading Type
T-Reference	-	Torsion
T30SF	30	Torsion
T60SF	60	Torsion
FC-Reference	-	Overhanging
FC-30SF	30	Overhanging
FC-60SF	60	Overhanging
F3-30SF	30	Three-point bending
F3-60SF	60	Three-point bending
F4-30SF	30	Four-point bending
F4-60SF	60	Four-point bending
AL-Reference-0	-	Axial load without eccentricity
AL-Reference-10	-	Axial load with 10 mm eccentricity
AL-Reference-20	-	Axial load with 20 mm eccentricity
AL-Reference-30	-	Axial load with 30 mm eccentricity
AL-30SF-0	30	Axial load without eccentricity
AL-30SF-10	30	Axial load with 10 mm eccentricity
AL-30SF-20	30	Axial load with 20 mm eccentricity
AL-30SF-30	30	Axial load with 30 mm eccentricity
AL-60SF-0	60	Axial load without eccentricity
AL-60SF-10	60	Axial load with 10 mm eccentricity
AL-60SF-20	60	Axial load with 20 mm eccentricity
AL-60SF-30	60	Axial load with 30 mm eccentricity

consist of two beams with 30 and 60 kg/m³ steel fibers under four-point bending (F4) and three-point bending (F3). However, the group, AL consists of twelve columns without and with 30 and 60 kg/m³ steel fiber under axial load without and with eccentric force. Three samples were produced from both column and beam samples, and the average of 3 samples is presented in tables and graphics.

2.2. Experimental setup

A universal testing machine with maximum capacity 1000 kN was used during the test program [29, 30]. The experimental setups are shown in Fig. 3. The experimental setup for torsion tests is a commonly used in literature [15, 31, 32]. The load was applied through a diagonal placed steel spreader beam. However, load was exposed incessantly in low rate and measured by a load cell and was applied as far as at the failure mode. The RC and SCRC beams are compared with each other by neglecting the frictional forces between the models and the setup. Two steel plates in the form of hollow boxes with a depth of 300 mm were used for both the right and left ends of the beams. As a rigid loading apparatus, 1460 mm HEB160 type steel profile was used in the experiments. The vertical load was applied to the central of HEB160 profile. Linear variable differential transformers (LVDTs) were used to measure displacements at different locations of the tested beams and to calculate the rotation at the beam subjected to pure torsion, as shown in Fig. 3a. Furthermore, the test set-up to apply bending moment is shown in Fig. 3.

As axial load is the main concern in the design of a column, the increasing axial force was applied during the experimental program to compare the effect of steel fibers with different eccentric loading. With the hydraulic jack with a capacity of 1000 kN, the load was applied to the columns in the vertical axis. For the columns without eccentricity, the load was applied from the center point of the 150x150 mm cross-section. In order to draw the interaction diagram in columns, it is necessary to calculate the bending moment as well as the axial load. In order to plot the axial load and moment interaction diagram, the vertical compressive load was applied to the cross sections of the columns. For the columns with 10, 20, and 30 mm eccentricity, the vertical load was applied at 10, 20, and 30 mm distance from the middle point of the column cross-section (Fig. 4). The axial force was applied with 0, 10, 20, and 30 mm eccentricity to draw the M-N interaction diagram. The column specimens were fixed from the lower and upper heads to the experimental setup. Thus, the columns are prevented from being moved horizontally for 10 cm. However, since the moment value, corresponding to the zero value of the normal force cannot be obtained experimentally, it was theoretically calculated according to the simple bending state (Eq-1). The axial load was increased up to the collapse mode in the columns, and the experiment was terminated.

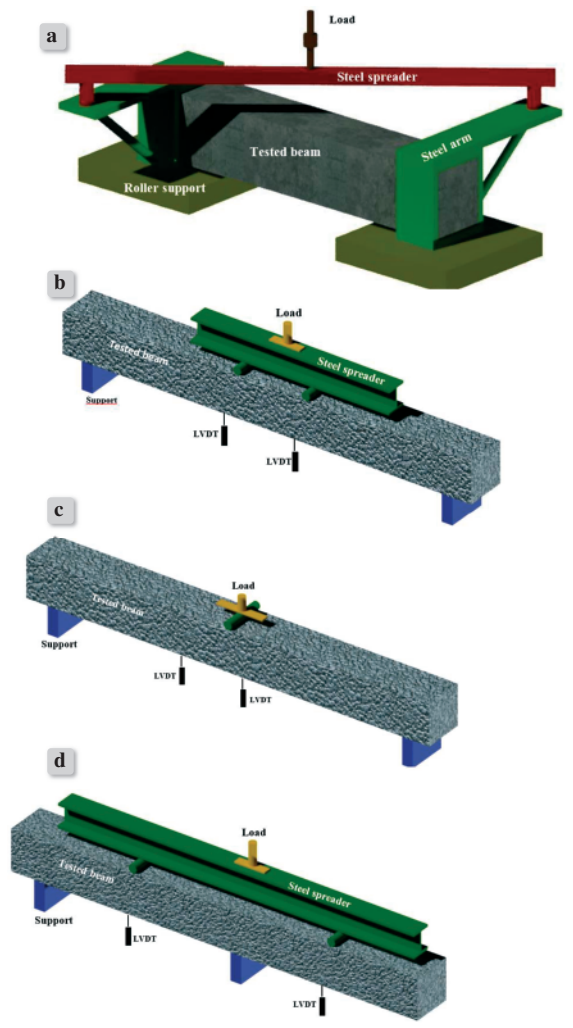The experimental setup to evaluate the eccentric loading behavior of the column is presented in Fig. 4.

Figure 3.
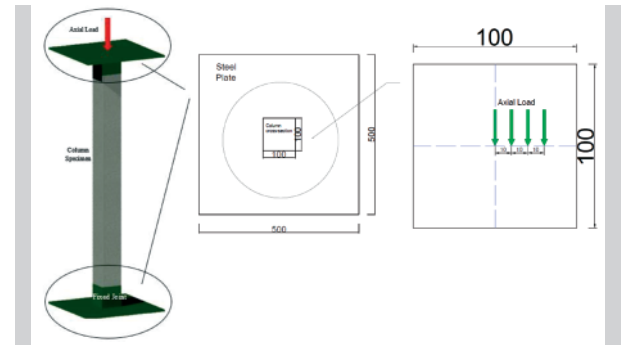**Test setup a) torsion b) four-point bending c) three-point bending d) overhanging**

Figure 4.
The test set-up of axial loading (all units are in mm)

$$M_r = M_0 = \left[0.85.f_{cd}.b.a.\left(d - \frac{a}{2}\right)\right] + \left[A_s^1.\sigma s^1(d - d^1)\right] \tag{1}$$

where M_r and M_o are flexural moment corresponding N = 0 axial load, f_{cd} is the concrete comprehensive strength (MPa), b and d, d' are the width and depth of column cross-section (mm), a is the effective depth, A_{s^1} is the area of longitudinal reinforcement (mm^2) and $\sigma s'$ is the yield strength of longitudinal reinforcement.
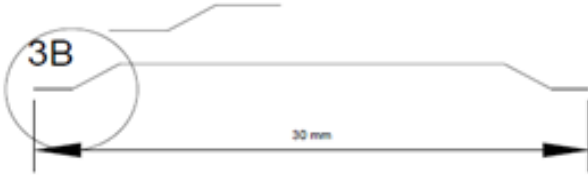
2.3. Materials and mixing

The concrete mix was designed using Portland Cement (CEM-I 42.5R), sand, water, fine and coarse aggregate. In the study, CEM I PC 42,5R cement was used in accordance with EN 197-1 [33] in all samples. Chemical, mechanical and physical properties of cement are given in Table 2. The cement used in manufacture of tested specimens was a locally manufactured general-purpose ordinary Portland Cement. The maximum size of coarse aggregate that is smaller than length and aspect ratio of the used steel fibers (40 mm) are chosen according to the RILEM TC 162 [34].

Table 2.
Chemical, physical and mechanical properties of the cement

Chemical properties (%)		Physical and mechanical properties	
SO_3	2.84	2 days Compressive strength (MPa)	27.90
MgO	2.58	28 days Compressive strength (MPa)	58.00
CaO	63.65	Initial setting time (min)	151
Al_2O_3	4.48	Final setting time (min)	191
K_2O	0.62	Specific gravity (g/cm^3)	3.12
SiO_2	18.10	Specific surface (cm^2/g)	3690
Na_2O	0.21	Total volume exp. (mm)	1.0
Fe_2O_3	3.09	Water requirement of cement (%)	29.5
CI-	0.015	Fineness (%)	7.15

Table 3.
Physical properties of steel fiber

Length (mm)	30	Tensile strength (MPa)	1100
Diameter (mm)	0.75	Aspect ratio	0.40

The sieve analysis of fine and coarse aggregate shown in Fig. 5 was performed according to the Turkish Standard TS 706 [35]. Dramix 3D steel hook fiber was used in the concrete mixture. The properties of the steel fibers are presented in Table 3.

Cement, sand, fine and coarse aggregates were dry-mixed for about 5 minutes and then water without plasticizer (2/3 volume of total water) was added gradually. Finally, the steel fibers were added very slowly in laboratory mixer and mixed for another 10 minutes to ensure sufficient workability and homogeneous fibers distribution. Water reducing admixture (BASF-Master Pozolith 530) of 1% by cement weight was used.

Table 4 shows the concrete mix proportions for plain and steel fiber concrete for all specimens. Before casting specified amount (30 and 60 kg/m³) of hooked steel fibers was added to the concrete mix and then the mixture was mixed for three minutes. The specimens were cured for 28 days at the laboratory conditions.

The values of 28-day compressive strength, flexural and tensile splitting concrete strengths and summary of test parameters of the beams and columns are presented in Table 4. During concrete mix, standard 100x200 mm cylinder samples were taken to calculate the compressive strength and tensile splitting strength and 100x100x270 mm prism samples were taken to calculate the bending strength. Uniaxial compression tests in accordance with the EN12390–3, splitting tensile strength in accordance with the EN12390-6 and flexural strength tests in accordance with the EN12390-5 were performed on cylinder and prism specimens for the 28 days. The splitting tensile and flexural strength of concrete are calculated using Eq.2. and Eq.3. respectively. Adding 30 and 60 kg of steel fiber to conventional concrete increased the tensile splitting strength by 3.42% and 32.1%, respectively. There has been a transfer of stress from the matrix to the fibers. Therefore, as the tensile strength of steel fibers is higher than that of concrete, the second and third groups have the higher tensile strength. However, it did not have a significant impact on the flexural strength. The addition of steel fiber reduced the flexural strength slightly. Similarly, increasing the steel fiber from 30 to 60 kg/m³ had no significant effect on the compressive strength. The addition of 30 kg and 60 kg steel fibers reduced the compressive strength by 4.1% and increased by 1.2%, respectively. After the concrete strength reached its maximum value, there was not much change in bending and compressive strength, especially due to the random distribution and discontinuity of the fibers to the matrix.

Table 4.
Concrete mixture

kg/m³	First Group	Second Group	Third Group
Fine aggregate (0–12mm)	1420	1420	1420
Coarse aggregate (12–28 mm)	510	510	510
Cement	320	320	320
Admixture	6.4	6.4	6.4
Steel fibers	-	30	60
Water/Cement ratio	0.31	0.31	0.31
Compressive strength (MPa)	34	32.6	34.4
Flexural strength (MPa)	59.0	58.3	58.6
Splitting tensile strength (MPa)	32.1	33.2	42.4

$$f_s = \frac{2P}{\pi a^2} \qquad (2)$$

$$f_l = \frac{PL}{bd^2} \qquad (3)$$

where f_s and f_l are the splitting tensile strength and flexural strength of concrete, respectively, a is the size of specimen, P is the applied load, L is the length of specimen and b and d are width and depth of prism.
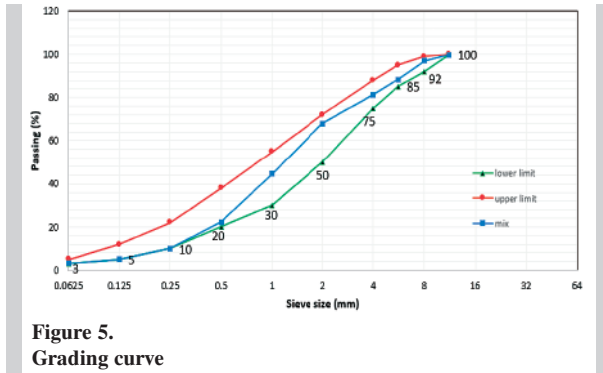

Figure 5.
Grading curve

3. TEST RESULTS

In this section, the behavior of tested beams under the torsional moment, bending moment and shear force and the behavior of tested column under axial load will be evaluated. It was evaluated under the headings of torsional behavior and bending and shear behavior and axial eccentric loading behavior. The ultimate torsion moment, the critical torsional moment (initial torsional moment valued corresponding to the initial crack), and the angles of rotation corresponding to these torsional moments are calculated. Torsional behavior was evaluated from the ultimate torsional moment-rotation angle. In addition, the crack formation and distribution were evaluated. Three and four-point bending tests were performed to evaluate flexural behavior, and an overhanging test to evaluate the shear behavior. Load-displacement graphs and the crack distributions of beams under bending and shear was investigated. Experimental values of beams under torsion, bending and shear were also compared with the empirical relations suggested by the relevant standards. Corresponding interaction diagrams were drawn by calculating the axial load and bending moment values of the columns.

3.1. Torsional behavior

The ultimate torsional moment (T_u), corresponding angle of twist per unit length (θ_u), torsional moment at cracking (T_{cr}), the angle of twist per unit length at

cracking (θ_{cr}), the corresponding angle of twist per unit length at yield point (θ_{yeld}) and torsional ductility index (μ_θ) of of tested beams under pure torsion are presented in Table 5. The post-cracking torsional response and the values of the ultimate torsional moment of the tested beams indicate that the steel fiber ratio plays a significant role in torsional moment capacity and corresponding angle of twist per unit length. The increase steel fiber ratio causes significant increase in torsional moment capacity and torsional ductility of tested beams. The values of the cracking torsional moment and the corresponding angle per unit length of the tested beams show that initial torsional response. T_u and θ_u values were obtained in the largest T60SF sample with 11.06 kNm and 5.58 deg/m respectively. The addition of 30 kg/m^3 and 60 kg/m^3 of steel fiber increased the T_u value by 39.6% and 105.95%, respectively, relative to the reference sample. Similarly, the addition of 30 kg/m^3 and 60 kg/m^3 of steel fiber increased the θ_u value by 20% and 118.8%, respectively, relative to the reference sample. The researchers reported that the addition of steel fiber contributed significantly in the increase the maximum resisting torque and maximum twist of RC beams under purer torsion [31, 32, 36]. The addition of steel fiber also increased torsional moment at cracking (T_{cr}) and the angle of twist per unit length at cracking (θ_{cr}). T_{cr} and θ_{cr} values were obtained with the largest T60SF sample with 0.60 kNm and 1.31 deg/m respectively. Hassan et all [37] showed that the additional of steel fiber increased the first cracking load. Table 5 shows that both RC beams with and without steel fiber under the torsional moment have reached most of the ultimate rotation capacity at the rotational value corresponding to the yielding moment. This behavior improves the insignificant effect of fibers on torsional moment capacity, which is mainly affected by shear reinforcement and the fibers have no shear strength enhancing the ability for the columns. Table 5 shows that both RC beams with, and without steel fiber under the torsional moment have reached most of the ultimate rotation capacity at the rotational value corresponding to the yielding moment. The addition of steel fiber showed its effectiveness after the rotation value at the time when the first crack occurred. The addition of 30 kg/m^3 steel fiber by volume did not have a significant enhancing effect on (θ_{cr}) and (θ_{yield}) values. However, doubling the fiber volume decreased the angle of rotation corresponding to the first crack, but significantly increased the value of the angle of

rotation and the ultimate angle of rotation. Nonetheless, the local fibers resisted to twist locally to enhance rotation capability. In this study, the torsional ductility index defined by Benardo and Lopez [38] was used. This index is defined as follow

$$\mu_\theta = \frac{\theta_u}{\theta_y} \qquad (4)$$

where θ_u is ultimate twist (corresponding to the ultimate torque T_u) and θ_y is yielding twist (corresponding to the yielding torque T_y). The experimental values for μ_θ are obtained from experimental T-θ curves. The highest torsional ductility index value is 1.30 at the T60SF. However, the torsional ductility index value of T60SF is higher than T-Reference and T60SF, 9.24% and 4.8%, respectively. Thus, the additional of steel fiber increased the torsional ductility index. Therefore, the T60SF specimen showed a ductile behavior than the others. In addition, the load value in which the initial crack is seen and the load values in which the final strength is reached indicate that the effectiveness of the fibers is especially effective when the behavior passes into the plastic region. The addition of steel fiber increased the torsional moment value corresponding occurred initial crack, but this increase was measured at very close values for the T30SF and T60SF. The first, secondary, and other diagonal torsional cracks formed under the effect of increased load after the first crack formed to tend to expand and progress. Hooked steel fibers were distributed randomly in the concrete section to prevent cracks from advancing and expanding. As the steel fiber volume increased, it also increased the amount of steel fiber and further limited the crack width. Instead of few and large crack widths, many cracks with smaller crack widths have occurred. This resulted in the ultimate torsional strength reaching the T60SF sample at maximum. However, in Table 5, the energy dissipation capacities were calculated from the area under the torsional moment-rotation angle curves (Fig. 6). It is evident that increasing of steel fiber reduces stiffness of the tested beams and therefore the increasing steel fiber increased the energy dissipation capacity of tested beams. The energy dissipation

capacity of T60SF beam specimen are higher than T30SF and T-Reference beam specimens, 171.29% and 355.24%, respectively. These phenomena can be explained by the result of continuity loss of concrete. However, the fibers perpendicular to loading direction improved the energy dissipation capacity by the adherence improvement of the fiber ends, also.

The relationship between the applied torque and the angle of twist per unit length is presented in Fig. 6. All the curves are for the mid span cross section. Until cracking the torsion moment-twist angle is relationship is nearly linear. After cracking the ultimate torsional moment significantly increases. After the cracking, at the same torsional moment levels the twist angle of T60SF specimen is higher than the others because of additional steel fiber. It has been shown that fibers randomly dispersed in concrete section collect the stresses themselves or transfer to undamaged areas after cracking. Based on the test results in Fig. 6 and Table 5, it was found that T60SF beam exhibits the best torsional behavior. The angle of the cracks plays a significant role in torsional strength of beams. As can be seen from Fig. 6, T60SF behaved better ductile than both T-Reference and T30SF. Compared with the beams with and without steel fiber, the addition of steel fiber played a significant role both for ultimate torsional moment capacity and corresponding angle of twist. As seen in Fig. 6, the increasing fiber ratio increased the torsional capacity, while increasing heterogeneity results increased twisting, while the torsional capacity is limited with continuing reinforcements, the noncontinuing fibers implies the minimal torsional capacity increase.
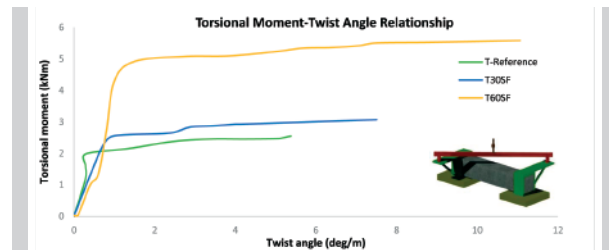

Figure 6.
Torsional moment-twist angle relationship

Table 5.
The Experimental results of torsional tests

Specimens	T_u (kNm)	θ_u (deg/m)	T_{cr} (kNm)	θ_{cr} (deg/m)	θ_{yeld} (deg/m)	μ_θ	Energy Dissipation Capacity (kN.deg)
T-Reference	5.37	2.55	0.29	1.60	2.14	1.19	12.02
T30SF	7.50	3.06	0.50	1.62	2.46	1.24	20.17
T60SF	11.06	5.58	0.60	1.31	4.30	1.30	54.72

Table 6.
The values defined by standards and experimental results

Specimens	T_{u-Exp}	$T_{u-mode\,II}$	Turkish Code TS 2018	American Code ACI318-19	European Code Eurocode-2 [39]	Australian Standard AS3600 [40]	British Standard BS8110	The ultimate torsional moment by Hsu [41]	The ultimate torsional moment by Rauch [42]
T-Reference	5.37	-						6.06	
T30SF	7.50	4.32	3.60	3.59	3.76	4.64	2.50	5.94	6.68
T60SF	11.06	4.44						6.10	

In order to investigate the accuracy of standards and empirical formulas of researchers for torsion, they are compared with the results. The experimental results are presented in Table 6 with the relevant standards for comparison. The $T_{Standard}/T_{Experimental}$ ratios are evaluated in Table 7. The discrepancy between the calculated and measured ones can be seen from Table 6 and 7. As seen, the best prediction for T-Reference specimen is given by the AS3600. The Turkish Standard and ACI318-19 calculated almost the same experimental and theoretical T_u values. The T_u values calculated according to relevant standards were less than the experimental one for no-fiber RC members. However, the theoretical ones proposed by Hsu and Rauch are greater than the experimental values. The T_u values of the beam with steel fibers were greater than the ones recommended by the standards. However, the T_u values proposed by Hsu and Rauch are close to ones of the samples with steel fibers, according to the standards. Table 7 indicates that the mentioned standards are insufficient to predict the T_u values of steel fiber reinforced RC members. Even with increasing steel fiber ratio, $T_{Standard}/T_{u-exp}$ ratio decreased. This is due to the fact that, the relevant standards consider the cross-section and reinforcement ratio, regardless of the concrete type, while calculating the torsional moment. Therefore, the post-cracking behavior of steel fiber reinforced concrete is neglected within the relevant standards. The reason, why there are three different values in the formula proposed by Hsu results from the fact that the author adds the elastic theory while calculating the Tu value. The elastic theory, while calculating the torsional moment, considers the tensile strength of the concrete as well as the cross-section of the member. The design procedure defined by AS3600, ACI318-19, and TS2018 supposes that the yielding of both horizontal and vertical reinforcements, and cross-section of the members affect the torsional moment. Nevertheless, these assumptions do not seem proper. The literature survey shows that, the yielding strengths of horizontal and vertical reinforcements are affected by the dimension, reinforcement ratio, and concrete comprehensive strength. Therefore, these mentioned standards ignore the effect of concrete comprehensive strength related to concrete tensile strength. Hence, the experimental ultimate torsional moments are different from the proposed ones, by standards.

Mansur [43] and Mansur and Paramasivam [36] carried out an experimental work on steel fiber reinforced concrete beams in bending, torsion and combined bending and torsion. They proposed two modes of failure to predict the torsional strength of steel fiber reinforced concrete beams as Mode 1 and Mode 2. Mode 2 that is modified as Eq-5, predicts the ultimate torsional strength of fiber reinforced concrete beams in pure torsion. Rauch assumed that both steel and concrete are elastic. The lateral reinforcement is to take the full amount of the principal tension, and all the bars at the section reach their yield stress. So ın the equation of Rauch, K constant was used $2\sqrt{2}$.

$$T_{u-mode\,II} = \frac{0.71b^2hf_r}{3} \qquad (5)$$

where $T_{u-mode\,II}$ is torsional strength by Mode II; b and h are width and depth of beam section respectively; f_r is modulus of rupture of concrete ($f_r = 0.8\sqrt{f_{cuf}}$) and f_{cuf} is fiber cube strength.

Table 7.
The comparison of experimental and numerical results

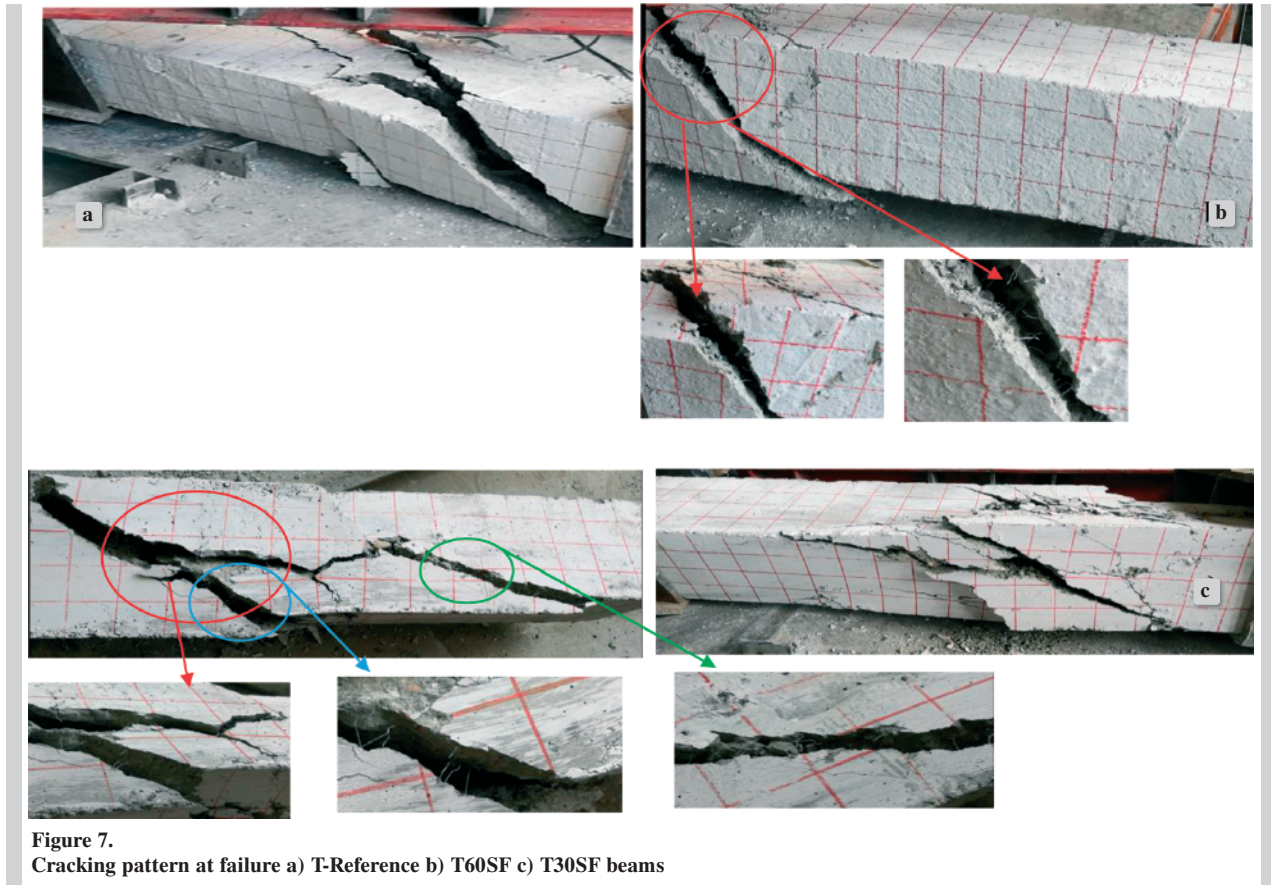| Specimens	T_{U-Exp}	$\frac{T_{u-mode\,II}}{T_{u-exp}}$	$\frac{T_{TS-2018}}{T_{U-Exp}}$	$\frac{T_{AC318-14}}{T_{U-Exp}}$	$\frac{T_{Eurocode-2}}{T_{U-Exp}}$	$\frac{T_{AS3600}}{T_{U-Exp}}$	$\frac{T_{BS8110}}{T_{U-Exp}}$	$\frac{T_{Hsu}}{T_{U-Exp}}$	$\frac{T_{Rauch}}{T_{U-Exp}}$
T-Reference	5.37	-	0.67	0.67	0.70	0.86	0.47	1.12	1.24
T30SF	7.50	0.58	0.48	0.48	0.50	0.62	0.34	0.79	0.89
T60SF	11.06	0.40	0.33	0.32	0.34	0.42	0.23	0.55	0.60

Figure 7.
Cracking pattern at failure a) T-Reference b) T60SF c) T30SF beams

Fig. 7 presents the crack patterns of the tested beams under pure torsion at failure. As seen, it can be observed that the beam without steel fiber "T-Reference specimen" exhibited more brittle torsional failure. The T-Reference specimen showed an abrupt collapse, and the cracks, firstly, occurred at the top section of the tested beam and separated suddenly by diagonal cracks. The first crack in the reference sample was observed as the torsional moment reached up to 2.73 kNm. Then, with the increased torsional moment, the crack spread rapidly and diagonally into the beam upper parts. The crack width is suddenly increased. Second, the cracks were formed after the post-cracking behavior. However, the widths of the secondary cracks were less than the first ones. The stiffness of the T-reference is decreased after the first crack. After cracking, the torsional behaviors of T30SF and T60SF were similar, because of steel fiber reinforcements in concrete. The first diagonal crack by torsional moment occurred at the higher load level for T30SF and T60SF than the T-Reference one.

The torsional behavior of T30SF and T60SF was different from the T-Reference. From Fig. 7, it can be seen that the average post-cracking torsional rigidity of T30SF and T60SF was greater than that of T-Reference, owing to the larger cracks related with high torsion. For the T30SF, the first crack was formed progressively, at the bottom part of the beam. However, the bottom crack for the reference member propagated till to support. With increasing load, the crack width increased more slowly than the reference sample. The first crack was formed at a torsional torque of 0.50 kNm. With the increased torsional moment, the second crack was observed in the mid-face of the beam. Then, the third crack was formed. After the cracks' propagation ended, the crack widths increased. The crack widths were measured by the fibers to a width less than the reference sample (Fig. 7c).

For the T60SF, the first crack occurred at a greater torsional moment than the T-Reference and T30SF. The first crack was observed near the head region of the beam. The crack width increased with increasing torsional torque. However, this increase was less than that of T-Reference and T60SF. In Fig. 7b and 7c, it is seen that, the steel fibers limit the crack width by bridging effect. The T60SF had a smaller number of second cracks than the T-Reference and T30SF sam-

ples. Further, the T60SF showed an increasing post-cracking behavior along with the formation of a number of diagonal cracks that became excessively wide as the imposed twist increased. As shown in Fig. 7, the steel fibers have a positive effect on torsional cracks. The addition of steel fiber has a significant effect on the level of the initial crack formation load and the behavior after crack formation. The crack propagation and the cracking explain the behavioral variations due to steel fibers and the loading type, which also implies the aim of this work from meso to macro scale. Amin and Bentz [44] and Patil and Sangle [45] showed that the addition of steel fiber reduced the crack spacing and crack width.

3.2. Flexural and shear behavior

Table 8 shows that the loading type also significantly affects the maximum deflection capacity. Free-end displacement was higher in 30 kg/m^3 beam groups compared to mid-point displacements in the overhanging test setup. In contrast, in the RC beams group with 60 kg/m^3 steel fiber, the highest maximum displacement was obtained from the 4-point bending test. The addition of steel fibers reduced the peak shear force and the shear force corresponding yielding point. However, this decrease was reduced by reducing the amount of steel fiber. The maximum shear force capacity of FC-Reference sample is 4% and 22.78% higher than FC-30SF and FC-60SF samples, respectively. Free end displacements are also reduced by adding steel fiber to the concrete. However, unlike the overhanging tests, in three and four-point bending tests, increasing the amount of steel fiber in the concrete mixture increased the maximum and shear strength values of RC beams. The maximum shear force of the F3-60SF and F4-60SF samples increased by 8.37% and 4.12%, respectively, compared to the F3-30SF and F4-30SF samples.

In the three-point bending test, due to the increase in the steel fiber ratio, the peak force increased with the bridging effect of the steel fibers, especially in the tensile zone of the beam. The principal tensile stresses in this region are met by steel fibers. In addition, the increase in the width of the cracks caused by the principal tensile stresses was prevented by the steel fibers. Thus, the peak deflection of the beam has been increased. Withal, the steel fiber did not have a significant effect until the yielding occurred in the reinforcement. Since the whole section is exposed to bending moment, the increase in the ratio of steel fiber could not delay the yield event in the reinforcement.

In the four-point bending test, the increasing steel fiber ratio was caused to increase the both yield and peak force due to lead the more continuous environment of the concrete sample. The randomly dispersed steel fibers increased the energy dissipation capacity and tensile strength of the samples (especially by improving the weak tensile strength of the plain concrete), due to its high elasticity. Thus, the increase in the fiber ratio increased the maximum deflection and yield deflection of the beams under shear and bending.

Table 8.
The values defined by standards and experimental results

Specimen	Yield force (kN)	Yield deflection (mm)	Peak force (kN)	Peak deflection (mm)
FC-Reference	170.02	3.31	267.95	37.58
FC-30SF	114.18	5.31	257.47	26.79
FC-60SF	132.31	5.51	218.24	12.52
F3-30SF	60.11	2.22	104.36	9.66
F3-60SF	73.51	1.74	113.10	12.80
F4-30SF	122.12	3.27	196.23	12.89
F4-60SF	128.13	4.53	204.37	20.11

For the shear force capacity, relevant empirical relations are presented in ACI318-19 and EuroCode-2. In related codes, it is expected that reinforced concrete beams are produced for conventional concrete. To the best of literature work, there is no formula presented for the shear capacity of fiber-reinforced concrete beams. The experimentally calculated maximum shear force values of steel fiber RC beams under shear force were compared with the empirical relations given by ACI318-19 and EuroCode-2. Table 9 shows the values of shear strength of tested beams and shear strength predictions based on the ACI318-19 and Eurocode-2 (EU2) equations. The shear strength is defined by ACI318-19 (ACI) (Eq-6, 7, and 8) and Eurocode-2 (EU2) (Eq-9,10, and 11) as follow:

$$V_{n-ACI} = V_{c-ACI} + V_{s-ACI} \qquad (6)$$

where V_n is the shear strength, V_{c-ACI} and V_{s-ACI} are the concrete strength and steel contribution, respectively, and equals to:

$$V_{c-ACI} = 0.158\sqrt{f_c}bd + 17.24\rho_w \frac{V_f d}{M_f}bd \le 0.29\sqrt{f_c}bd \qquad (7)$$

$$V_{s-ACI} = \frac{A_{sw}f_{yv}d}{s} \qquad (8)$$

where f_c and f_{yv} are the concrete comprehensive strength (MPa) and yield strength of longitudinal reinforcement (MPa), respectively, b and d are the

Table 9.
The experimental results

Specimens	$V_{u\text{-}Exp}$ (kN)	$V_{n\text{-}ACI}$ (kN)	$\dfrac{V_{(n\text{-}ACI)}}{V_{(u\text{-}Exp)}}$	$V_{n\text{-}EU2}$ (kN)	$\dfrac{V_{(n\text{-}EU2)}}{V_{(u\text{-}Exp)}}$	Energy Dissipation Capacity (kNmm)
FC-Reference	267.95	64.89	0.24	72.84	0.27	1302.7
FC-30SF	257.47	64.19	0.25	72.84	0.28	5726.1
FC-60SF	218.24	65.09	0.30	72.84	0.33	1122.3
F3-30SF	104.36	64.19	0.62	72.84	0.70	266.3
F3-60SF	113.10	65.09	0.58	72.84	0.64	226.4
F4-30SF	196.23	64.19	0.33	72.84	0.37	887.6
F4-60SF	204.37	65.09	0.32	72.84	0.36	1313.8

width and depth of beam (mm), A_{sw} is the area of stirrup (mm^2), s is the spacing of stirrup (mm), ρ_w is reinforcement ratio, V_f and M_f are the factor shear and moment at section, respectively.

$$V_{n-EU} = V_{Rd,c} + V_{Rd,s} \qquad (9)$$

$$V_{Rd,c} = \left[0.18\left(1 + \sqrt{200/d}\right)(100\rho_w f_{ck})^{1/3}\right]b_w d \qquad (10)$$

$$V_{n-EU} = V_{Rd,c} + V_{Rd,s} \qquad (11)$$

where ρ_w is the longitudinal reinforcement ratio, f_{ck} is the concrete comprehensive strength ($=f_c$), (MPa), f_{ywd} is the design yield strength of stirrup (MPa).

Table 9 reports that the values of experimental shear strength are very much than the values defined by ACI and EU2. By comparing the experimental and predicted shear strength, it appears that both ACI (Eq-6) and EU2 (Eq-9) underestimate the strength of tested beams with and without steel fiber. As it can be seen from Table 9, the values are lower than those obtained experimentally. The flexural strength tests were performed on beams at 28 days in accordance with the EN 12390-5 [46] and RILEM TC 162 TDF [34].
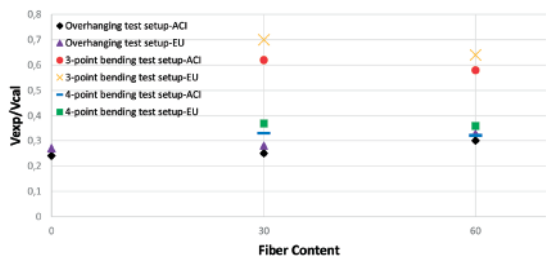

Figure 8.
Influence of shear index on the shear capacity of beams by different codes

As can be seen from Table 9 and Fig. 8, the steel fibers increased the shear strength of tested beams for three and four-point bending test. The maximum increase in the shear strength of the beam specimens with steel fiber was achieved for the three-point bending loading. However, increasing the steel fiber ratio decreased the shear strength of tested beam specimens for the overhanging beam. Increasing the steel fibers from 30 to 60 kg/m^3 for the four-point bending and three-point bending tests, increased the shear strength by 4.15% and 8.37%; whereas increasing the steel fiber ratio from 0 to 30 kg/m^3 and from 30 to 60 kg/m^3 in the overhanging beam decreased the shear strength by 3.9% and 15.23%, respectively. It is concluded that the steel fiber plays an important role in shear strength at the loading type of overhanging beam. However, the steel fiber content has a little effect on the shear strength for three and four-point bending tests. The fiber inclusion decreased the shear strength gain for the shear type testing with the cantilever system, the energy dissipation capacity is observed as the maximum not for the specimens with maximum fibers, but with the FC-30SF (Fig. 9). While the fibers perpendicular to loading direction improved the energy dissipation capacity by the adherence improvement of the fiber ends, the lack of continuity of the fibers decreased the shear strength. Thus, as a practical way of energy dissipation capacity comparison, the area below the load-displacement curves is used to evaluate the energy dissipation capacities of the samples. As expected, all above-mentioned implications are the characteristic values, which will be replaced with design parameters according to relevant standards within the design process. The results from experiments yields higher peak loads partly due to steel fibre reinforcement that is not considered in the current codes and partly due to the fact that the experimental results tend to be around average carrying capacity while codified design calculations are based on significantly lower design values level.
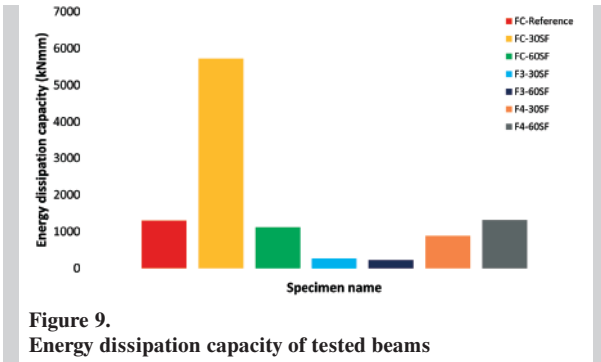
Figure 9.
Energy dissipation capacity of tested beams

Figure 10.
Load displacement relationship a) three-point and b) four-point bending c) overhanging beam

The experimental load-displacements curves are shown in Fig. 10. It can be seen from load-displacement curves that the loading type and fiber content has a significant effect on the flexural behavior. The vertical displacements were recorded at mid-span between the support for four-point and three-point bending and at the free end for overhanging beam. The midpoint displacements are neglected because the midpoint displacements of tested beams under overhanging are smaller, when compared to the free end displacements. In Fig.10a and b, the midpoint displacements are plotted as the average of the values recorded from the two LVDTs located in the middle region of the beam. However, in Fig. 10c, the values of free end displacements, and are plotted by using the LVTD values that were located at the free end of the beam. As can be seen from Fig. 10a and 10b, the F3-30SF sample exhibited a more rigid behavior than the others. Fig. 10c shows that the beam without steel fiber (FC-Reference specimen) behaved more ductile than the ones with steel fiber. The displacement capacity of the beams decreased with increasing steel fiber ratio. Increasing the steel fiber ratio from 0 to 30 kg/m³ decreased the free-end displacement by about 15%. The overhanging beam loading type and increasing the steel fiber ratio from 30 to 60 kg/m³, in comparison with the reference specimen, decreased the free-end displacement by about 4% and 23%, respectively. When the FC-30SF and FC-60SF specimens are compared, similar free-end displacement decreasing was observed. Changing the loading system at the same fiber ratio (comparison with F3-30SF and F4-30SF) resulted in a significant reduction in both shear strength and displacement capacity. The shear strength and midpoint displacement capacity of the F3-30SF was obtained more than the F4-30SF by about 31% and 108%, respectively. It has been concluded that changing the loading system from three and four point bending to overhanging beam has a significant effect on shear strength.
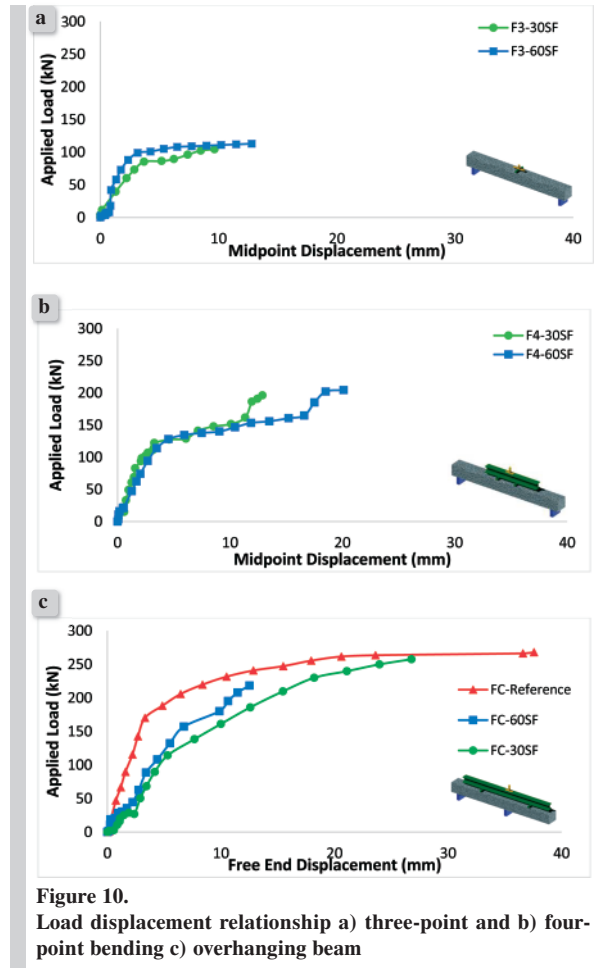
By comparing the F3-30SF and F4-30SF with the FC-30SF, the shear strength increased by about 60% and 24%, respectively. Similarly, the shear strength of the samples with 60 kg/m³ steel fibers increased for overhanging type-loading system. Sturm et all. [47] carried out a numerical/analytical study to evaluate the effect of steel fiber on the shear capacity of RC beams. The results of this study show that additional of fibers can improve the shear capacity. Moreover, the researchers [48–50] reported that the addition of steel fiber to the conventional concrete increased the shear capacity of RC beams. The discontinuity of fibers resulted in decreasing strength of the shear type specimens as expected, while the steel reinforcement describes the general behavior.

The photographs of tested beams are presented in Fig. 11 to evaluate the effect of the additional steel fiber on the crack occurrence, propagation and distribution at failure. The experimental evidence showed that the different crack propagation and patterns occurred depending on the loading system and
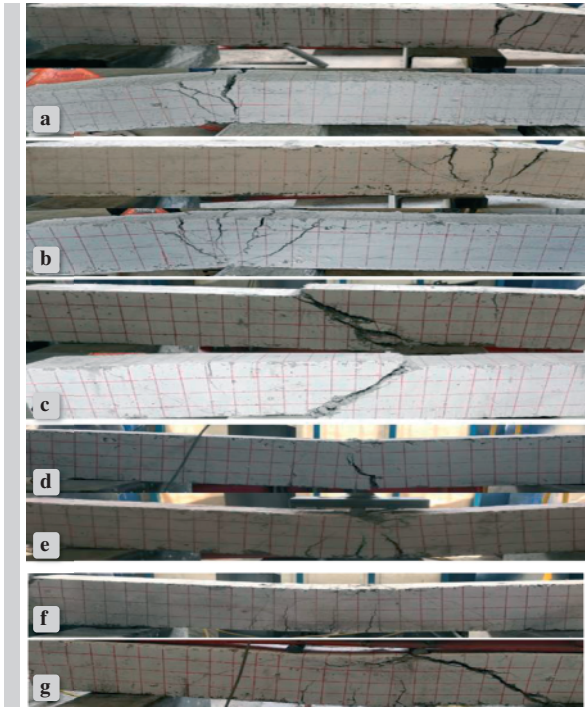
Figure 11.
Crack pattern at failure a) FC-Reference b) FC-30SF c) FC-60SF d) F3-30SF e) F3-60SF f) F4-30SF g) F4-60SF

steel fiber ratio, as expected. Withal, the failure modes are observed as expected for relevant experiments as shear; just near the support of hanging beam and bending about the mid-section of the samples.

Unlike the three and four-point loading tests for the FC-Reference sample, the first crack was formed at the support upper face, at free-end side of the beam. The crack width of the first crack increased with increasing shear force. The second crack was also formed at near the free-end and near the first crack. At 200 kN, the width of the cracks increased at the free-end side (Fig. 11a). The loading system for shear (overhanging beam), increasing the fiber ratio from 0 to 30 kg/m^3 resulted in a reduction in crack widths and resulted in an increase in the number of cracks (Fig. 11b). The energy required to occur the first crack in RC beams without steel fiber is less than RC beams with steel fiber. Since the steel fibers carry to the stress, the energy required for spreading of the crack increases. Therefore, the crack widths of the RC beams without fiber are less than the RC beams with fiber, but the number of cracks is higher. Nevertheless, the higher increase of the steel fibers results increasing heterogeneity, which implies the decreasing strength values after an ultimate point. The first crack was formed on the support on the

free-end side, similar to the FC-Reference sample. Unlike FC-Reference and FC-30SF samples, the first crack was formed between two supports in the FC-60SF specimen with a shear test type. The reason for this difference is thought to be due to the activity of the steel fibers at the free-end. A second crack was formed on the free-end support at approximately 150 kN (Fig. 11c). For the F3-30SF specimen, the first cracking was observed when the shear force reached about 60 kN. The first crack occurred in the lower midpoint and the lower region of the beam. With increasing shear force, the crack continued along the beam height. With the shear force reaching approximately 80 kN, the crack width of the first crack increased, and the second crack was formed in the mid-section of the beam. However, at the end of the experiment, the width of the second crack was not as large as the first crack, as expected. Shear strength before reaching the V_u value, cracks with a much smaller crack width were formed in the upper section of the beam, then the first and second cracks. In the F3-60SF sample, the first crack was observed at a shear force of about 67 kN. When we compare the F3-SF60 with the F3-SF30 sample, the observed shear force of the first step for both samples is almost the same. A larger number of smaller but smaller crack widths were observed in the F3-60SF sample at the time of the experiment. The first crack was formed in the mid-section of the beam similar to the F3-SF30 sample and advanced along the height of the beam. When the shear force reached up to 113.10 kN, the experiment was completed (Fig. 11e). There were spalling, when the shear force reached approximately to 105 kN. For the F4-30SF sample, the first crack formed approximately at 110 kN. However, the first crack was also observed in the lower and middle region of the beam. With increasing shear force, the crack advanced along the beam height at the shear force of about 130 kN. The third and the fourth cracks were formed with the second crack with increasing load in the mid-section of the beam. Although the number of cracks was greater than the F3-30SF sample, the crack widths were measured at smaller values (Fig. 11f). The first crack in the F4-60SF was observed at 120 kN. It was predicted that the first crack occurs at greater shear values relative to F3-30SF, F3-60SF, and F430SF samples, both increasing fiber ratio and changing the loading type. However, similar to other samples, the first crack was formed in the middle and lower region of the beam. As the shear force increased to approximately 190 kN, spalling and crushing were observed in the upper section of the beam (Fig. 11g).

3.3. Axial eccentric loading behavior

Three specimens (with and without steel fibers) were tested for axial loading and nine RC specimens (with and without steel fiber) were subjected to eccentric loading with 10, 20, and 30 mm eccentricity. The interaction diagrams obtained from the experiments provide an improved understanding of the cross-section behavior of RC column with steel fibers, when subjected to axial load. For design purposes of columns subjected to different loading conditions, an experimental axial load-bending moment interaction diagram (N-M) was drawn based on the test results. The ultimate axial loads and the ultimate bending moments of the RC columns were tested under concentric and eccentric loading (10 mm, 20 mm, and 30 mm). The N-M diagram was constructed from five points. The first point represents the ultimate axial load obtained from the specimens tested under concentric loading. The second, third and fourth points substitute for the ultimate eccentric axial loads at 10 mm, 20 mm and 50 mm, respectively. The fifth point corresponds to the ultimate bending moment that represented the ultimate flexural load obtained from specimens tested under flexural loading. Furthermore, since the fifth point, the bending moment corresponding to the zero value of the normal force (N = 0), cannot be obtained experimentally, it was theoretically calculated according to Eq-1.

The failure mode of columns occurred in the form of crushing of concrete in the upper and bottom part of the column and with the yielding of longitudinal reinforcement. The results show that increasing the steel fiber content increased both axial load and moment capacity. Fig. 12 shows the interaction diagram of column with and without steel fiber. Although increasing the steel fiber ratio from 0 to 30 kg/m³ and from 30 to 60 kg/m³ decreased the axial load and moment capacity. The energy dissipation capacity of the column with 30 kg/m³ steel fiber was the highest one, as expected according to Fig. 12. However, the formation of the first crack was observed of the latest specimen during testing because of the increasing steel fiber content. It is seen that although the steel fiber content increased, the moment and axial load capacity increased (Fig. 12). Furthermore, the fiber content increase had a positive effect on ductility, while it did not have a significant effect on strength. Increasing the steel fiber ratio from 0 to 30 kg/m³ and from 0 to 60 kg/m³ increased the axial load capacity by about 7% and 1%, respectively and increased the moment capacity by about 8% and 1%, respectively. Some assumptions made for the construction of the interaction diagram for RC columns, however, need to be addressed by experimental research, such as the amount, aspect ratio or volume ratio of steel fiber, which was taken here in order to produce results on the safe side.
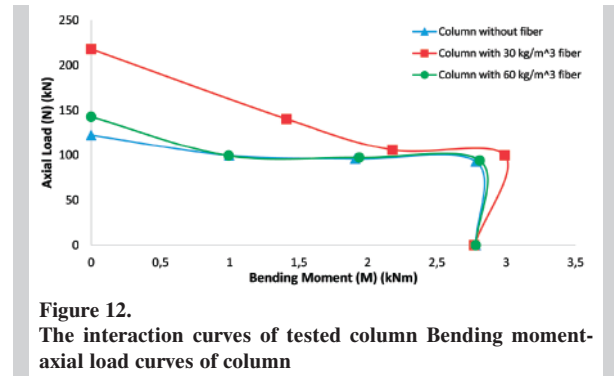

Figure 12.
The interaction curves of tested column Bending moment-axial load curves of column

Table 12 presents the experimental ultimate axial loads and the corresponding ultimate moments of the tested specimens under concentric, eccentric loading. It was observed that all the specimens that were subjected to eccentric loading have exhibited crushing of the concrete cover at the compression face at reaching the ultimate load carrying capacity, as expected. The pure compression occurred at M = 0 kNm and N = 122.6 kN load level in the column specimen without steel fiber. In this case, all column cross-sections are subjected to the compressive force and crushing concrete was observed during testing. The pure compression occurred at M = 0 kNm and N = 217.9 kN load level in the column specimen with 30 kg/m³ steel fiber. For the column specimens with 60 kg/m³ steel fiber, the pure compression was occurred at M = 0 kNm and N = 142.9 kN load level. In this paper in which the effect of the steel fiber amount on column load carrying capacity was investigated, increasing the steel fiber amount had a positive effect on loading capacity. Increasing the steel fiber amount from 0 to 30 kg/m³ and from 30 kg/m³ to 60 kg/m³ increased the loading capacity by 54% and 10%, respectively. It has been observed that although increasing the steel fiber amount increased the load carrying capacity compared to the reference column specimen (without steel fiber), this relationship did not continue in most likely. The steel fibers in the RC column delayed the early spalling of the concrete cover which resulted in an increase in the load carrying capacity of the RC columns.

Table 10.
Ultimate load and moment values of tested columns

Group	Specimen	Ultimate Load (kN)	Ultimate Moment (kNm)
	AL-Reference-0	122.6	0
	AL-Reference-10	99.6	0.99
Concentric	AL-Reference-20	95.7	1.91
	AL-Reference-30	92.8	2.77
	Theoretical Result	0	2.78
	AL-30SF-0	217.9	0
	AL-30SF-10	140.5	1.41
Eccentric	AL-30SF-20	105.9	2.12
	AL-30SF-30	99.7	2.99
	Theoretical Result	0	2.78
	AL-60SF-0	142.9	0
	AL-60SF-10	99.2	0.99
Eccentric	AL-60SF-20	97.1	1.94
	AL-60SF-30	93.8	2.81
	Theoretical Result	0	2.79

Figure 13.
The columns after tests

Data from the Table 10 shows that adding 60 kg/m^3 of steel fiber has increased the axial load carrying capacity by a small portion; but reducing the amount of steel fiber by 2 times has significantly increased the axial load carrying capacity. Axial load carrying capacity of AL30SF-0 and AL-60SF-0 samples increased by 77.7% and 16.6%, respectively, compared to AL-Reference-0 sample. As expected, the increase of the eccentricity, decreased the axial load carrying capacity. This decrease in axial load carrying capacity was obtained as 24.3%, 54.2% and 34.3%, respectively, for the fiber reinforced samples of 30 and 60 kg/m^3. The lack of continuum for concrete section by fibers decreased the axial load carrying capacity.

Fig. 13 shows the pictures of the columns that have reached the fracture failure mode under axial load. Fracture in the columns occurred in the lower and upper head regions.

4. CONCLUSION

An experimental investigation of behavior of beams without and with steel fiber subjected to torsion and shear and the behavior of columns without, and with steel fibers subjected to axial load is presented. Test variables, which adopted major factors, are the amount of steel fiber (0, 30 and 60 kg/m^3), loading type (torsion, axial load and shear force consisted of three different types of bending moment namely three and four-point bending and overhanging beam). Overall ten beams and ten columns were test-ed (three beams under pure torsion, seven beams under shear force and 10 columns under axial load). The results of this study indicate the following concluding remarks.

1. Without steel fiber, the brittle behavior associated with diagonal failure was observed in torsional testing.

2. The torsional moment capacity of tested beams is affected by the amount of steel fiber. Increasing steel fiber amount played a significant role on the torsional moment capacity. However, T60SF beam specimen reached the highest torsional moment capacity and corresponding angle of twist; probably due to the steel fibers take the stresses around the cracks themselves. Compared to the beams without and with steel fiber, increasing of the amount of steel fiber from 0 to 30 kg/m^3 and from 30 kg/m^3 to 60 kg/m^3 causes energy dissipation capacity and ductility index increasing by 67.8%, 171.35 and 4.2%, 4.8%, respectively. Further the beam with 60 kg/m^3 steel fiber under pure torsion reached the highest torsional moment at cracking and the angle of twist per unit length at cracking.

3. The torsional moment capacities are defined by the provisions of current codes, such as ACI318-19, Eurocode-2, British, Australian and Turkish Standards. However, these codes are based on the experimental results of beams with conventional

concrete, without fiber. Hence, the shear and torsional moment capacity of the beams with steel fiber need to be compared to the values that are defined by codes, which underestimate the torsional moment capacity of the tested beams without and with steel fibers.

4. The beam specimen without steel fiber reached the highest shear strength capacity. On the other hand, the loading type for shear force is affected to the shear strength and displacement capacity. However, the displacement capacity of the beams decreased with increasing steel fiber ratio. Increasing the fiber ratio from 0 to 30 kg/m^3, decreased the free-end displacement by 14.68%. At the overhanging loading type, increasing the steel fiber ratio by 30 and 60 kg/m^3 decreased the free-end displacement by 3.91% and 22.77% in comparison with the reference specimen, respectively.

5. It appears that the code provisions cannot predict the shear strength capacity of tested beams without and with steel fiber.

6. The increase in the fiber ratio did not cause a significant increase in axial load capacity. However, the flexural strength and energy dissipation capacity increased due to effectiveness of the fibers in bending, for the eccentric loaded members. While the fibers perpendicular to loading direction improved the energy dissipation capacity by the adherence improvement of the fiber ends, the lack of continuity of the fibers decreased the relevant strength.

7. The ultimate load decreased, and the ultimate moment increased with the increase of eccentricity for all column specimens. İncreasing the steel fiber amount had a positive effect on loading capacity. Increasing the steel fiber amount from 0 to 30 kg/m^3 and from 30 kg/m^3 to 60 kg/m^3 increased the loading capacity by 54% and 10%, respectively. The energy dissipation capacity of the column with 30 kg/m^3 steel fiber was the highest one.

8. The shear strength and the torsional moment capacities are defined by the provision of current codes of practice such as ACI318-19, Eurocode-2, British, Australian and Turkish Standards. However, these codes are based on the experimental results for conventional concrete, without fiber. Hence, the shear and torsional moment capacity of beams with steel fiber need to be compared to the values that are defined by codes. The

standards underestimate the predicted shear and torsional moment capacity of tested beams without and with steel fiber.

ACKNOWLEDGMENT

REFERENCES

[1] Patil, S.P. and K.K.J.J.o.B.E. Sangle, (2016). Tests of steel fibre reinforced concrete beams under predominant torsion. *Journal of Building Engineering*, 6, 157–162.

[2] Aydın, A.C., Bayrak B., (2019). The torsional behavior of reinforced self-compacting concrete beams. *Advances in Concrete Construction, 8*(3), 187–198.

[3] Mertol, H.C., E. Baran, and H.J. Bello, (2015). Flexural behavior of lightly and heavily reinforced steel fiber concrete beams. *Construction and Building Materials*, 98, 185–193.

[4] Aydin, A.C., Karakoccedil, M. B., Düzgün, O. A., & Bayraktutan, M. S. (2010). Effect of low quality aggregates on the mechanical properties of lightweight concrete. *Scientific Research and Essays, 5*(10), 1133–1140.

[5] Türkmen, I., Öz, A., & Aydin, A.C. (2010). Characteristics of workability, strength, and ultrasonic pulse velocity of SCC containing zeolite and slag. *Scientific Research and Essays, 5*(15), 2055–2064.

[6] Baran, E., Akis, T., & Yesilmen, Y. (2012). Pull-out behavior of prestressing strands in steel fiber reinforced concrete. *Construction and Building Materials, 28*(1), 362–371.

[7] Guler, S., Yavuz, D., Korkut, F., & Ashour, A. (2019). Strength prediction models for steel, synthetic, and hybrid fiber reinforced concretes. *Structural Concrete, 20*(1), 428–445.

[8] Huang, H., Yuan, Y., Zhang, W., & Zhu, L. (2020). Experimental study on the mechanical properties and the microstructure of hybrid fiber reinforced concrete under an early stage. *Structural Concrete, 21*(3), 1106–1122.

[9] Chalioris, C.E. & Karayannis, C. G. (2009). Effectiveness of the use of steel fibres on the torsional behaviour of flanged concrete beams. *Cement and Concrete Composites, 31*(5), 331–341.

[10] Nanni, A. (1991). Fatigue behaviour of steel fiber reinforced concrete. *Cement and Concrete Composites, 13*(4), 239–245.

[11] Karayannis, C.G. (2000). Nonlinear analysis and tests of steel-fiber concrete beams in torsion. *Structural Engineering and Mechanics, 9*(4), 323–338.

[12] Karayannis, C.G. & Chalioris, C.E. (2000). Experimental validation of smeared analysis for plain concrete in torsion. *Journal of Structural Engineering, 126*(6), 646–653.

[13] Rao, T.G. & Seshu, D.R. (2003). Torsion of steel fiber reinforced concrete members. *Cement And Concrete Research, 33*(11), 1783–1788.

[14] Sucharda, O., Pajak, M., Ponikiewski, T., & Konecny, P. (2017). Identification of mechanical and fracture properties of self-compacting concrete beams with different types of steel fibres using inverse analysis. *Construction and Building Materials*, 138, 263–275.

[15] Pawlak, W. & Kamiński, M. (2012). Cracking of reinforced concrete beams under torsion—theory and experimental research. *Archives Of Civil And Mechanical Engineering*, 12, 368–375.

[16] Barghlame, H., & Lotfollahi-Yaghin, M. A. (2011). Investigating the capacity of ultimate torsion of concrete prismatic beams with transverse spiral bars. World Academy of Science, Engineering and Technology, *International Journal of Civil, Environmental, Structural, Construction and Architectural Engineering, 5*(11), 561–566.

[17] Yang, I.-H., Joh, C., Lee, J. W., & Kim, B. S. (2013). Torsional behavior of ultra-high performance concrete squared beams. *Engineering Structures*, 56, 372–383.

[18] Deifalla, A. & Ghobarah, A.J.E.S. (2014). Behavior and analysis of inverted T-shaped RC beams under shear and torsion. *Engineering Structures*, 68, 57–70.

[19] ACI-318-19, (2019). Building Code Requirements for Structural Concrete and Commentary. American Concrete Institute: Farmington Hills, MI, USA.

[20] EuroCode-2, (1991). Design of Concrete Structures. Part 1: General Rules and Rules for Buildings. European Committee for Standardisation: European Prestandard, CEN, Brussels.

[21] Code, T.B.S., Specification for Structures to be Built in Seismic Zones 2018, Ministry of Public Works and Settlement: Ankara, Turkey.

[22] Bernardo, L., Andrade, J. & Lopes, S. (2012). Softened truss model for reinforced NSC and HSC beams under torsion: A comparative study. *Journal Engineering Structures*, 42, 278–296.

[23] Caldas, R.B., Sousa Jr, J.B.M. & Fakury, R.H.J.E.S. (2010). Interaction diagrams for reinforced concrete sections subjected to fire. *Engineering Structures, 32*(9), 2832–2838.

[24] Law, A. & Gillie, M.J.E.S. (2010). Interaction diagrams for ambient and heated concrete sections. *Engineering Structures, 32*(6), 1641–1649.

[25] Pham, D.T., de Buhan, P., Florence, C., Heck, J. V., & Nguyen, H. H. (2015). Interaction diagrams of reinforced concrete sections in fire: *A yield design approach. Engineering Structures*, 90, 38–47.

[26] Lechman, M. (2016). Resistance of reinforced concrete columns subjected to axial force and bending. *Transportation Research Procedia*, 14, 2411–2420.

[27] DBYBHY, (2018). Turkish seismic code.

[28] ACI/Committee318. (2014). Building Code Requirements for Structural Concrete (ACI 318–14): An ACI Standard: Commentary on Building Code Requirements for Structural Concrete (ACI 318R-14): an ACI Report.American Concrete Institute.

[29] Korucuk, F.M.A., Maali, M., Kılıç, M., & Aydın, A. C. (2019). Experimental analysis of the effect of dent variation on the buckling capacity of thin-walled cylindrical shells. *Thin-Walled Structures*, 143, 106259.

[30] Maali, M., Kılıç, M., Yaman, Z., Ağcakoca, E., & Aydın, A. C. (2019). Buckling and post-buckling behavior of various dented cylindrical shells using CFRP strips subjected to uniform external pressure: Comparison of theoretical and experimental data. *Thin-Walled Structures*, 137, 29–39.

[31] Facconi, L., Minelli, F., Ceresa, P., & Plizzari, G. (2021). Steel fibers for replacing minimum reinforcement in beams under torsion. *Materials and Structures, 54*(1), 1–18.

[32] Lee, J.-Y., Haroon, M., Shin, D., & Kim, S. W. (2021). Shear and torsional design of reinforced concrete members with high-strength reinforcement. *Journal of Structural Engineering, 147*(2), 04020327.

[33] EN197-1, Cement Part 1: Composition and conformity criteria for comonn cement in Turkey 2002: Turkish Standart.

[34] RILEM, RILEM TC 162-TDF: (2001). Test and design methods for steel fibre reinforced concrete-Uni-axial tension test for steel fibre reinforced concrete. 34(235), 3–6.

[35] TS706, Aggregates for concrete (written in Turkish). 1998, Turkish Standards Institute: Ankara, Turkey.

[36] Mansur, M. & Paramasivam, P. (1985). Fiber reinforced concrete beams in torsion, bending, and shear. Journal Proceedings.

[37] Hassan, R.F., Jaber, M. H., Al-Salim, N. H., & Hussein, H. H. (2020). Experimental research on torsional strength of synthetic/steel fiber-reinforced hollow concrete beam. *Engineering Structures*, 220, 110948.

[38] Bernardo, L.F. & Lopes, S.M. (2009). Torsion in High-Strength Concrete Hollow Beams: Strength and Ductility Analysis. *ACI Structural Journal, 106*(1).

[39] EN, B., 1-2: 2004 Eurocode 2: (2004). Design of concrete structures-Part 1-2: General rules-Structural fire design. European Standards, London.

[40] AS, A.S., Concrete structures. (2001). AS3600-2001. Sydney (Australia): Standards Australia.

[41] Hsu, T.T., (1968). Torsion of Structural Concrete-Plain Cocnrete Rectangular Sections. *Special Publication*, 18, 203-238.

[42] Csikós, Á. & Hegedûs, I. (1998). Torsion of reinforced concrete beams. Technical University of Budapest, Department of Reinforced Concrete Structures H- Budapest.

[43] Mansur, M. (1982). Bending–torsion interaction for concrete beams reinforced with steel fibres. *Magazine of Concrete Research, 34*(121), 182–190.

[44] Amin, A. & Bentz, E.C. (2018). Strength of steel fiber reinforced concrete beams in pure torsion. *Structural Concrete, 19*(3), 684–694.

[45] Patil, S.P. & Sangle, K.K. (2016). Tests of steel fibre reinforced concrete beams under predominant torsion. *Journal of Building Engineering,* 6, 157–162.

[46] TS12390-5, T.E., (2002). Testing hardened concrete-part 5: Flexural strength of test specimens. Turkish Standard.

[47] Sturm, A., Visintin, P. & Oehlers, D. (2021). Mechanics of shear failure in fiber-reinforced concrete beams. *Journal of Structural Engineering, 147*(3), 04020344.

[48] Amin, A. & Foster, S.J. (2016). Shear strength of steel fibre reinforced concrete beams with stirrups. Engineering Structures, 111, 323-332.

[49] Aoude, H., Belghiti, M., Cook, W. D., & Mitchell, D. (2012). Response of steel fiber-reinforced concrete beams with and without stirrups. *ACI Structural Journal, 109*(3).

[50] Conforti, A., Minelli, F. & Plizzari, G.A. (2013). Wide-shallow beams with and without steel fibres: a peculiar behaviour in shear and flexure. *Composites Part B: Engineering*, 51, 282–290.